Hijacking of host negative regulator RIOK3 by a fish virus orchestrates stealthy subversion of interferon immunity

Can Zhang[a,c,#], Long-Feng Lu[a,c,#], Ming-Kun Yang[a,c], Chu-Jing Zhou[a,e], Hui-Lin Li[a,c], Bao-jie Cui[a,e], Zhuo-Cong Li[a,c], Yang-Yang Wang[a,c], Zhen-Qi Li[a,c], Xiao Xu[a,e], Meng-Ze Tian[a,c], Feng-Xiong[a,c], Dan-Dan Chen[a,c], Li Zhou[a,c], Shun Li[a,b,c,d,e,2,*] ,Feng Ge[a,c,*]

[a]Key Laboratory of Breeding Biotechnology and Sustainable Aquaculture, Institute of Hydrobiology, Chinese Academy of Sciences, Wuhan, Hubei 430072, China

[b]Laboratory for Marine Biology and Biotechnology, Qingdao Marine Science and Technology Center

[c]University of Chinese Academy of Sciences, Beijing, China

[d]Key Laboratory of Aquaculture Disease Control, Ministry of Agriculture, Wuhan, China

[e]College of Fisheries and Life Science, Dalian Ocean University, Dalian, China

***Corresponding authors Email:**

Feng Ge: gefeng@ihb.ac.cn

Shun Li: bob@ihb.ac.cn

[#]The authors contributed equally to this work.

Keywords: fish virus, immune escape, RIOK3, interferon

Abstract

Viruses commonly evade host immunity by directly targeting and destroying positive regulators of interferon (IFN) signaling. Here, we reveal an indirect and stealthy immune evasion strategy employed by a fish virus, whereby the Spring Viraemia of Carp Virus (SVCV) phosphoprotein (P protein) antagonizes host IFN responses by upregulating the host negative regulator RIOK3. Proteomics analysis identified significant upregulation of the kinase RIOK3 upon SVCV infection. We demonstrate that fish RIOK3 negatively regulates type I IFN by recruiting the selective autophagy receptor p62 to mediate degradation of TBK1. Furthermore, the SVCV P protein stabilizes RIOK3 protein levels through the E3 ubiquitin ligase TRIM11. Functional assays confirmed that the inhibition of IFN by the P protein is enhanced by RIOK3 overexpression and significantly diminished upon RIOK3 knockdown. Our findings uncover a mechanism where SVCV P protein hijacks the host negative regulator RIOK3 to suppress IFN production indirectly, representing an efficient and stealthy viral immune evasion strategy.

Significance Statement

Here, we describe a stealth immune evasion mechanism of Spring Viraemia of Carp Virus (SVCV). Instead of directly targeting positive regulators, the viral phosphoprotein (P protein) stabilizes the host negative regulator RIOK3 via the E3 ubiquitin ligase TRIM11, which in turn promotes the autophagic degradation of TBK1 and attenuates type I interferon (IFN) responses. This work reveals an indirect strategy through which the fish virus exploits the host negative regulatory protein to avoid antiviral immunity.

Introduction

Viral infection triggers the rapid induction of type I interferons (IFNs) and interferon-stimulated genes (ISGs), establishing an intracellular antiviral state (1, 2). In the evolutionary arms race with the hosts, viruses have developed diverse strategies to directly antagonize this IFN response (3–5). For instance, mammalian viruses, such as Herpes simplex virus 1(HSV-1) inhibits TANK-binding kinase (TBK1) by forming the Us11-Hsp90 complex, thereby inactivating IFN (6). SARS-CoV-2 Nsp8 suppresses MDA5-mediated IFN antiviral immune responses by disrupting the K63-linked polyubiquitination process mediated by TRIM4 (7). Similarly, fish viruses utilize direct targeting strategies: Cyprinid herpesvirus 2 (CyHV-2) kinase-like protein (KLP) degrades STING via a Beclin1-dependent autophagy pathway (8). Grass Carp Reovirus (GCRV) VP41 reduces STING phosphorylation by acting as a decoy substrate of TBK1, effectively dampening the host IFN response (9). These established mechanisms predominantly involve viral direct destruction of core positive regulators within the IFN signaling pathway, representing a conspicuous and readily detectable form of immune evasion. Beyond strategies that directly target host positive regulators, how viruses exploit host negative regulators and the underlying molecular mechanisms represents a promising frontier for investigation.

Following viral RNA sensing by cytoplasmic RIG-I-like receptors (RLRs), the MAVS–STING–TBK1 signaling axis is sequentially activated, leading to phosphorylation of IRF3/7 and initiation of IFN transcription (10–13). To prevent immunopathological damage from uncontrolled IFN production and cytokine storm, hosts employ intricate negative feedback mechanisms (14). The IFN negative regulatory system is recognized as indispensable components for maintaining immune homeostasis. Multiple negative regulatory factors (e.g., SOCS1/TRIM13/PIAS1) have been identified in mammals (15–17). And over the past decade, several such factors have also been discovered in fish, including IRF10, TMEM33, and CDK2 (18–20). Functionally, host IFN

66 negative regulation and viral immune evasion share the common outcome of suppressing IFN
67 production. However, host negative regulation is an intrinsic physiological process that typically
68 operates without eliciting overt cellular toxicity, such as premature apoptosis. Therefore, it is
69 worthy of reflection whether viruses can exploit these existing host negative regulatory
70 mechanisms to achieve immune evasion indirectly.
71 The serine/threonine kinase RIOK3 belongs to the evolutionarily conserved RIO kinase family,
72 which comprises four members: RIOK1, RIOK2, RIOK3, and RIOKB. Accumulated evidence
73 indicates that the RIO family participates in the regulation of innate immune responses. For
74 example, RIOK-1 has been reported to act as a suppressor of the p38 MAPK innate immune
75 pathway in *Caenorhabditis elegans* (21). RIOK3 is found only in multicellular eukaryotes and has
76 been implicated in apoptosis and ribosomal quality control (22–25). In mammals, the immune-
77 regulatory role of RIOK3 remains controversial: some studies propose that RIOK3 negatively
78 regulates MDA5 via the RLR signalling axis, thereby suppressing type I IFN production (26, 27),
79 whereas Feng et al. observed that RIOK3 interacts with TBK1 and IRF3 to promote IFN induction
80 (28). In fish, previous studies have reported that Yellow catfish (*Pelteobagrus fulvidraco*) RIO
81 kinases (RIOKs) negatively regulate IFN signaling, however, the underlying molecular mechanism
82 remains unclear and its functional connection to viral immune evasion remains entirely unexplored
83 (29).
84 Spring Viraemia of Carp Virus (SVCV), a major pathogen of cyprinid fish, is a single-stranded
85 negative-sense RNA virus encoding five proteins (30, 31). In this study, we establish that RIOK3
86 serves as a key negative regulator of the fish IFN pathway. We further demonstrate that the SVCV
87 phosphoprotein (P protein) specifically upregulates host RIOK3 expression to mediate suppression
88 of IFN production. These findings reveal a covert strategy in vertebrate virus by hijacking an
89 intrinsic immunoregulatory system to achieve immune evasion, highlighting the use of an indirect
90 and stealthy strategy to subvert host defenses.

91

Results

1. Proteomics identifies RIOK3 involved in antiviral immunity

SVCV is a highly virulent pathogen of cyprinid fish, causing mortality within 48 h of infection and possessing exceptional immune evasion capabilities. To investigate the underlying immune evasion mechanism, we employed fish cells infected with SVCV as a model (Figure 1A). Partial cell aggregation occurred at 6 h, lesions increased at 24 h, and detachment expanded by 48 h (Figure 1B and 1C). Viral titers rose progressively (Figure 1D). To gain a clear understanding of the dynamic process of SVCV infection, we analyzed changes in protein abundance at four time points using label-free quantitative proteomics (Figure 1E). Label-free quantitative proteomics identified 5,467 proteins, with 5,245 quantifiable across replicates. Among these, 1,774 were differentially expressed (DEPs), with only 16 common across all time points (Figure 1F-1H). Figures S1 and S2 show the Gene Ontology (GO) classification and Kyoto Encyclopedia of Genes and Genomes (KEGG) enrichment analysis of the DEPs. We selected RIOK3, from among the 12 upregulated proteins, for further investigation and Parallel Reaction Monitoring (PRM) validation (Figure 1I and 1J). To validate the RIOK3 expression pattern indicated by proteomic data, we assessed its transcription in zebrafish liver following infection with SVCV. Infection induced substantial upregulation of riok3 (Figure 1K). A similar increase was observed across multiple fish cell lines, including those derived from zebrafish, gibel carp, and grass carp, supporting a conserved role for RIOK3 in antiviral responses (Figure 1L). These findings suggest that RIOK3 contributes to antiviral immunity during SVCV infection.

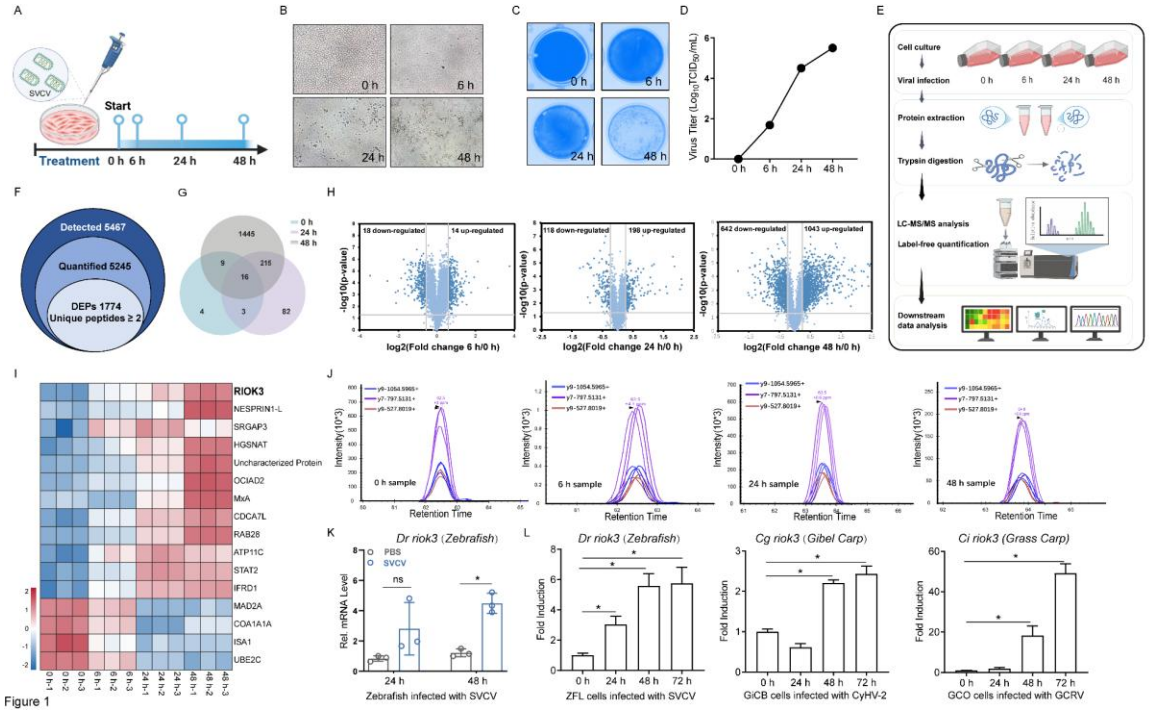

Figure 1

Figure 1. Proteomics identifies RIOK3 involved in antiviral immunity. (A) A model for adding SVCV to EPC cells. (B) Cells uninfected (0 h) or infected with SVCV (MOI = 1) for 6 h, 24 h, and 48 h were analyzed microscopically. (C) EPC cells uninfected or infected with SVCV at 6 h, 24 h, and 48 h were fixed with 4% paraformaldehyde (PFA) for 1 h and stained with crystal violet to observe the cytopathy. (D) Titer assay of cells infected with SVCV for 6 h/24 h/48 h. (E) Processes for label-free quantitative proteomics. (F) Characterize the number of proteins detected, quantified and differentially expressed proteins in proteomics. (G) Wayne plots characterizing differentially expressed proteins at 6 h, 24 h, and 48 h post-infection. (H) Volcano plots of the distribution of up- and down-regulated differentially expressed proteins at 6 h, 24 h, and 48 h after infection with SVCV. (I) The heatmap shows the expression of DEPs common to the three time points. The labels "-1", "-2", and "-3" represent the three technical replicates corresponding to this experiment. The raw log_2-transformed expression values for the 16 DEPs featured in Figure 1I across all time points are provided in Supplementary Table S1. (J) Fragment ion extraction-ion chromatograms (XIC) representing representative peptides of RIOK3 at different time points after infection with SVCV. (K) PBS or SVCV (5×10^8 $TCID_{50}$/mL, 5 μL/each) was administered intraperitoneally to zebrafish (3 per group), and liver tissues were harvested at 24 h/48 h. qRT-PCR was conducted to detect the expression of *riok3*. In the statistical analysis of the annotated data, $p < 0.05$ is considered to indicate a significant difference.(L) ZFL cells, GiCB cells, and GCO cells were cultured in 6-well plates with SVCV (MOI = 1), CyHV-2 (MOI = 0.0001) and GCRV (MOI = 1000). Total RNA was extracted at 0 h, 24 h, 48 h, and 72 h, *Dr riok3*, *Cg riok3,* and *Ci riok3* were detected by qRT-PCR.

2. RIOK3 promotes SVCV proliferation *in vivo*

To further validate the role of RIOK3 in antiviral immune responses, we generated zebrafish mutants lacking a functional *riok3* gene and confirmed the successful knockout of *riok3* (Figure

S3). Firstly, a significantly higher survival rate for *riok3*$^{-/-}$ zebrafish compared to wild-type (WT) when infected with SVCV (Figure 2A). The liver, spleen, and heart tissues were collected 48 h after injection of SVCV, and viral components were analyzed (Figure 2B). As illustrated in Figure 2C and 2E, the transcription and expression of SVCV N in the liver and spleen were found to be significantly lower in the *riok3*$^{-/-}$ group. Furthermore, IFN expression was higher in the livers of *riok3*$^{-/-}$ zebrafish than in WT zebrafish (Figure 2D). Heart tissue from the infected WT zebrafish showed the highest viral titer (Figure 2F). Based on this, we assayed heart tissue and found that *riok3*$^{-/-}$ mutants exhibited a lower viral titer (Figure 2G). The extent of damage to liver and spleen tissues in the *riok3*$^{-/-}$ group was less severe (Figure 2H). Furthermore, immunofluorescence (IF) assay revealed a significant reduction in the green fluorescent signal of the SVCV N protein in the *riok3*$^{-/-}$ group (Figures 2I). Overall, the viral load was significantly reduced in *riok3*$^{-/-}$ zebrafish following SVCV infection.

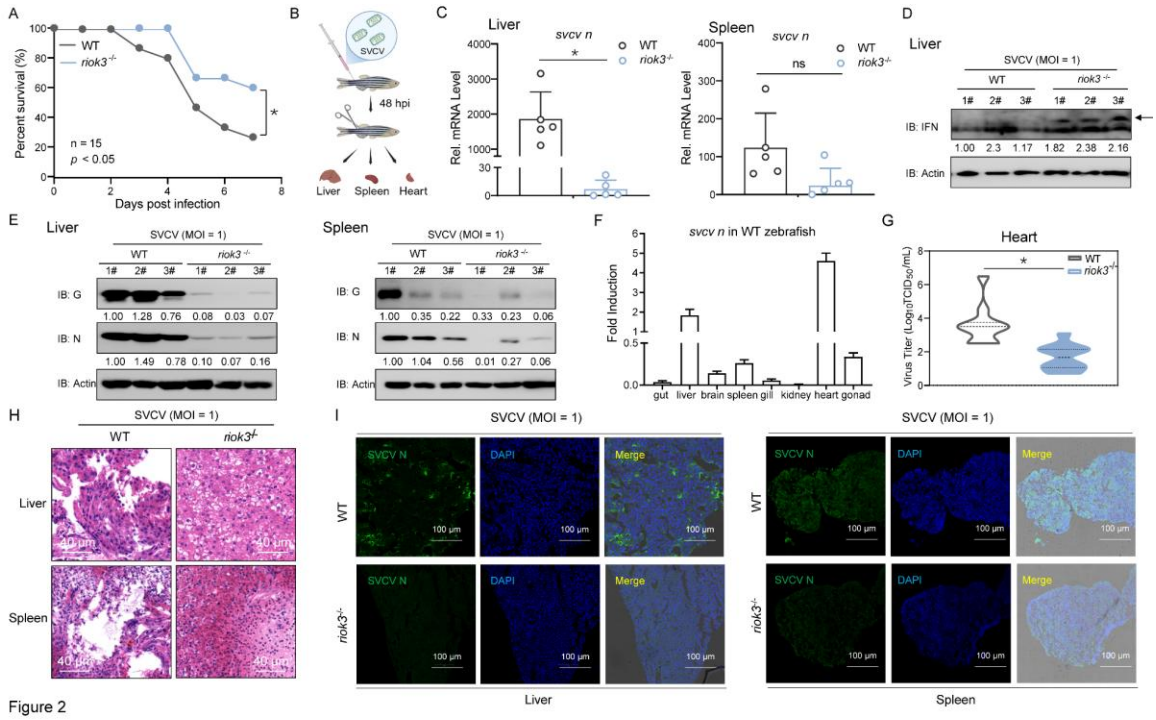

Figure 2

Figure 2. RIOK3 promotes SVCV proliferation *in vivo*. (A) SVCV (5×10^8 $TCID_{50}$/mL, 5 μL/each) was

injected into WT zebrafish and *riok3*$^{-/-}$ zebrafish (15 per group), respectively, and survival was counted on a daily basis (Kaplan-Meier curves). (B) Schematic diagram of tissue dissection 48 h after zebrafish infection with SVCV. (C) qRT-PCR analysis of svcv-*n* mRNA in the liver and spleen of WT and *riok3*$^{-/-}$ zebrafish (n = 5 per group) given i.p. injection of SVCV for 48 h. (D and E) Immunoblotting (IB) analysis of SVCV proteins in the liver and spleen sections of WT and *riok3*$^{-/-}$ zebrafish (n = 3 per group) treated with SVCV for 48 h. (F) qRT-PCR detection of viral load in various tissues of WT zebrafish after infection with SVCV. (G) Viral loads were detected in the hearts of WT and *riok3*$^{-/-}$ zebrafish (15 per group). (H) After treating WT and *riok3*$^{-/-}$ zebrafish with SVCV (5×10^8 $TCID_{50}$/mL, 5 μL/each) for 72 h, H&E-stained liver and spleen sections were observed microscopically. (I) Fluorescent microscopy images of liver and spleen tissue sections from SVCV-infected zebrafish (WT and *riok3*$^{-/-}$ groups) were acquired using a confocal microscope (SP8; Leica) with a 20× objective lens (n = 5 per group, 3 non-overlapping sections per fish). Green fluorescence represents proliferation of the SVCV envelope protein N. Scale bar, 100 μm. In the statistical analysis of the annotated data, $p < 0.05$ is considered to indicate a significant difference.

3. RIOK3 promotes SVCV proliferation *in vitro* and negatively regulates IFN expression

Next, we examined the influence of RIOK3 on SVCV replication *in vitro*. As shown in Figure 3A, overexpression of RIOK3 upregulated the transcription of SVCV genes (*p*, *n*, and *g*). We designed short hairpin RNAs (shRNAs) targeting RIOK3 and confirmed that sh-*riok3*#1 yielded the most efficient knockdown (Figure 3B). Knockdown of *riok3* suppressed viral gene expression (Figure 3C). Consistently, RIOK3 overexpression increased viral protein levels, whereas *riok3* knockdown reduced them (Figure 3D and 3E). Furthermore, RIOK3-overexpressing cells displayed more pronounced cytopathic effects (CPE) and higher viral titers following SVCV infection, whereas *riok3* knockdown attenuated these responses (Figure 3F and 3G). IF analysis revealed enhanced SVCV N and P protein signals upon RIOK3 overexpression (Figure 3H and 3I). Conversely, SVCV N and P protein signals were attenuated following *riok3* knockdown (Figure 3J and 3K). Together, these results demonstrate that RIOK3 enhances viral replication *in vitro*.

Given the critical role of the IFN system in innate antiviral immunity, we next asked whether RIOK3 modulates host IFN responses. Overexpression of RIOK3 suppressed the activation of the IFN1 promoter and the IFN-stimulated response element (ISRE) following stimulation, whereas *riok3* knockdown enhanced their activation (Figure 3L and 3M). Similarly, RIOK3 overexpression inhibited the transcription of *ifn* and *isg15-1*, while *riok3* knockdown led to their upregulation

(Figure 3N and 3O). These data suggest that RIOK3 facilitates SVCV replication by antagonizing the host IFN response.

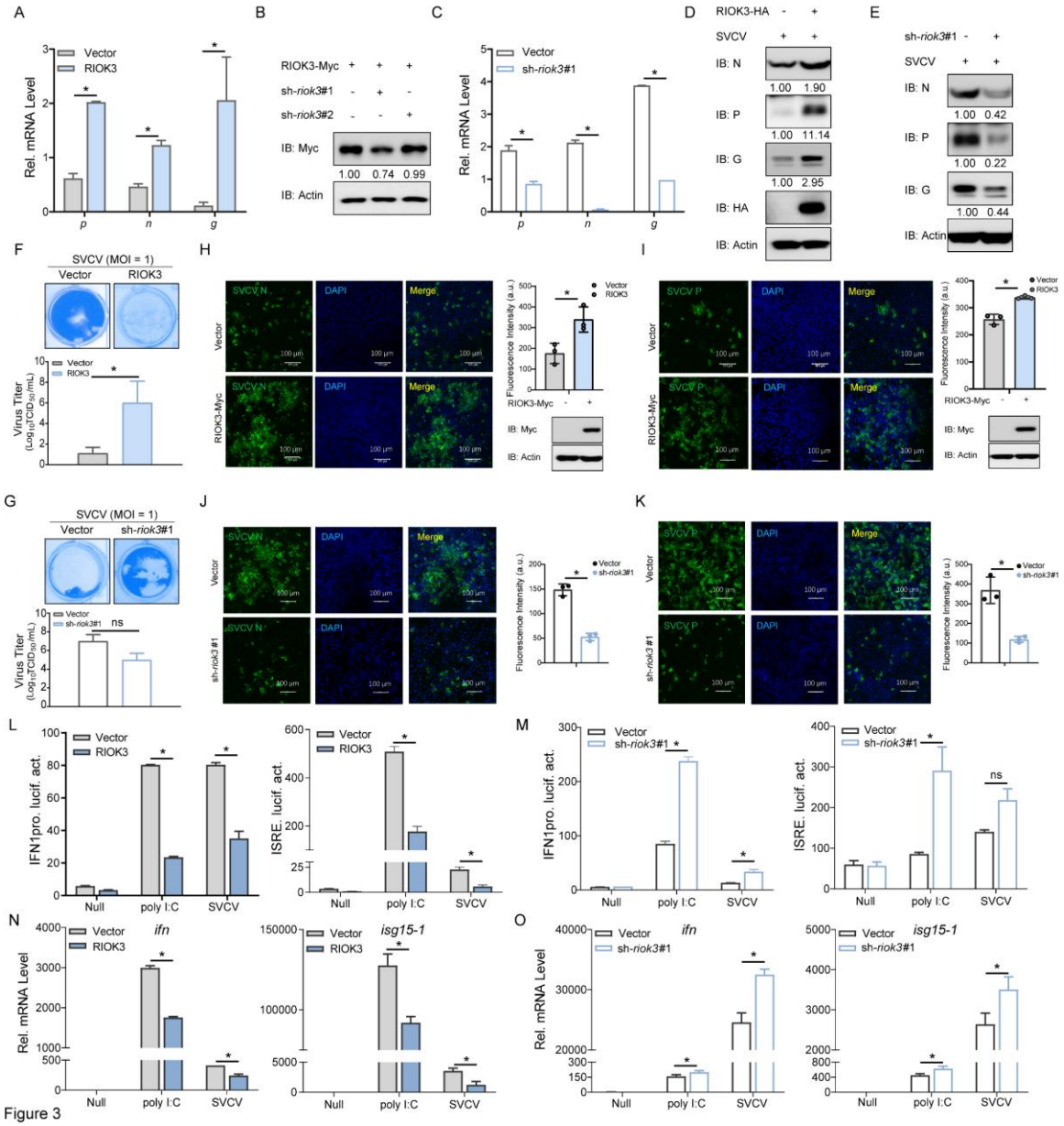

Figure 3

Figure 3. RIOK3 promotes SVCV proliferation in vitro and negatively regulates IFNexpression. (A and C) qRT-PCR analysis of SVCV genes in EPC cells transfected with indicated plasmids (1 μg) for 24 h, followed by SVCV challenge for 24 h. (B) IB analysis to validate the RIOK3 knockdown effect in EPC cells transfected with the indicated plasmids (1 μg). (D and E) IB analysis of the effects of overexpressing 1 μg RIOK3 (sh-*riok3*#1) on the N/P/G proteins of the SVCV virus. (F and G) After 24 h of transfecting 1 μg RIOK3-Myc/sh-*riok3*#1 into EPC cells, the cells were infected with SVCV, followed by observation of CPE, plaque assay, and titer determination. (H-K) The effect of

overexpression 1 μg RIOK3 (or sh-*riok3*#1) on SVCV was analyzed by IF. N and P proteins were observed under a 20× immersion objective (SP8; Leica). Scale bar, 100 μm. (L and M) 24 h after transfection of EPC cells with the diagrammed plasmid (0.25 μg RIOK3-Myc/sh-*riok3*#1, 0.25 μg IFN1pro-Luc/ISRE, 0.05 μg TK), cells were transfected with poly I:C (0.5 μg) or infected with SVCV (MOI = 1) for 24 h. Finally, luciferase activity for IFN1promoter and ISRE was detected using a luciferase assay. (N and O) qRT-PCR analysis of *ifn* and *isg15-1* in EPC cells transfected with indicated plasmids (1 μg) for 24 h, and then infected with SVCV (MOI = 1) or transfected with poly I:C (0.5 μg) for 24 h.

4. RIOK3 inhibits the IFN response by promoting TBK1 degradation

We next sought to elucidate the mechanism through which RIOK3 suppresses IFN expression. KEGG enrichment analysis indicated that the RIG-I-like receptor (RLR) signaling pathway was the most significantly enriched immune-related pathway among proteins upregulated at 24 h post-infection with SVCV (Figure 4A). Consistent with this, heatmap analysis revealed marked upregulation of key molecules associated with the RLR pathway (Figure 4B). Overexpression of RIOK3 inhibited IFN1 promoter and ISRE activation induced by TBK1, but not by MAVS (Figure 4C). Conversely, knockdown of *riok3* rescued TBK1-mediated activation of the IFN response (Figure 4D). Co-immunoprecipitation (co-IP) assays confirmed an interaction between RIOK3 and TBK1 (Figure 4E), and confocal microscopy demonstrated their colocalization in the cytoplasm (Figure 4F). We further evaluated whether RIOK3 affects TBK1 protein levels. Overexpression of RIOK3 led to a reduction in TBK1 expression (Figure 4G). Similarly, RIOK3 suppressed endogenous TBK1 levels following SVCV infection or poly I:C stimulation. However, knock down *riok3* abolished this inhibitory effect (Figures 4H and 4I). Confocal imaging corroborated these findings, showing attenuated TBK1 fluorescence signal in cells overexpressing RIOK3 (Figure 4J). Together, these results indicate that RIOK3 negatively regulates the type I IFN response by facilitating the degradation of TBK1.

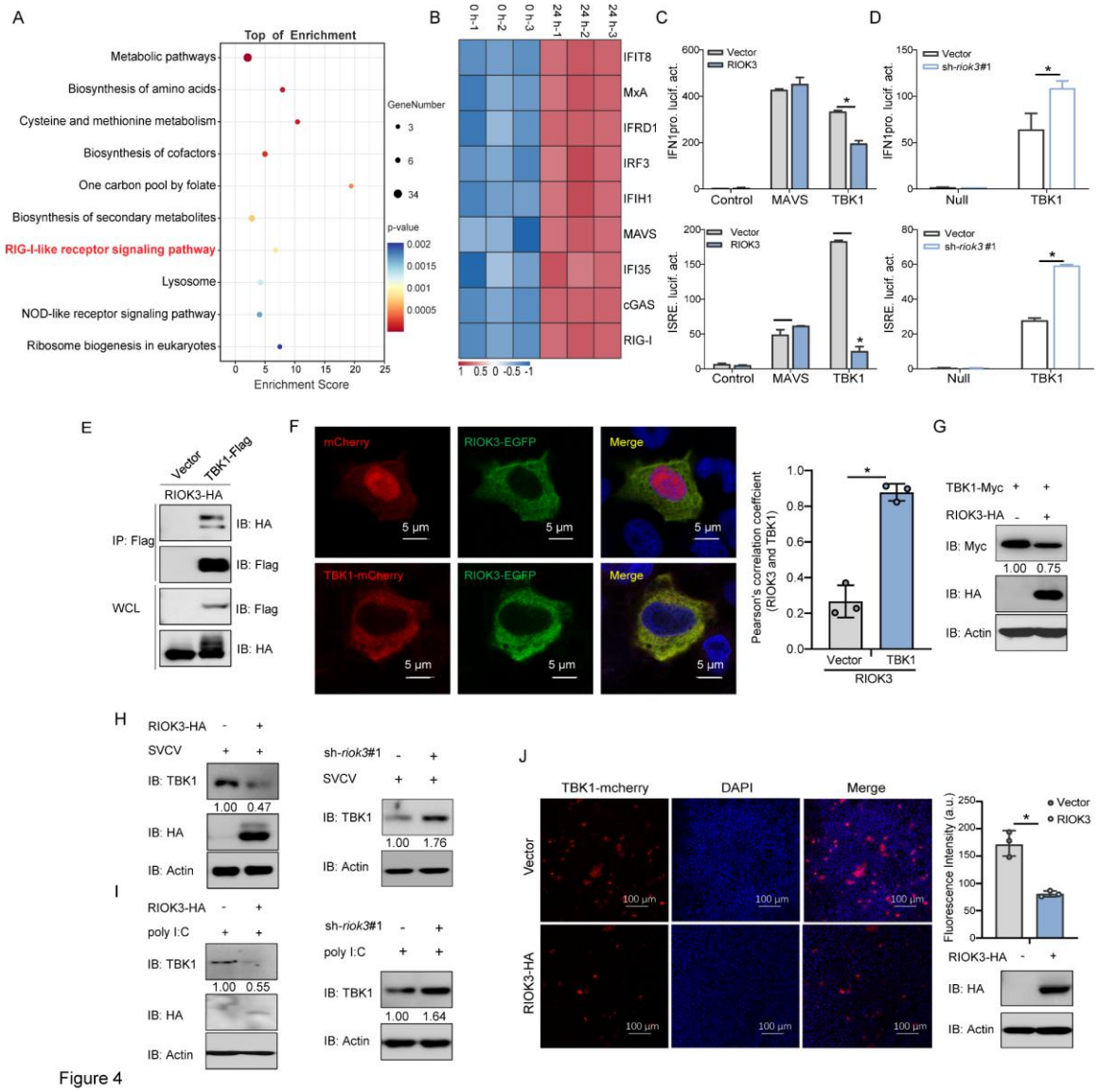

Figure 4

Figure 4. RIOK3 inhibits IFN response by degrading TBK1. (A) Top 10 signaling pathways for differentially expressed proteins (DEPs) upregulated at 24 h in KEGG enrichment analysis. (B) Heatmap of RLR-associated protein changes in EPC cells 24 h after SVCV infection. The labels "-1", "-2", and "-3" represent the three technical replicates corresponding to this experiment. (C and D) EPC cells were cultured in 24-well plates for 24 h before transfection with the indicated plasmid (0.25 μg RIOK3-Myc/sh-riok3#1, 0.25 μg IFN1pro-Luc/ISRE, 0.25 μg MAVS/TBK1-Myc, 0.05 μg TK). 24 h later, IFN1pro and ISRE activity was monitored using luciferase assays. (E) EPC cells were cultured in 10 cm^2 dishes and transfected with the described plasmids (5 μg each). 24 h later, cell lysates were immunoprecipitated using an anti-Flag affinity beads. The immunoprecipitants and whole cell lysates (WCLs) were then probed with Abs for IB analysis. (F) EPC cells were cultured onto coverslips of 6-well plates and transfected with RIOK3-EGFP and TBK1-mCherry/mCherry (1 μg each). 24 h later, cells were fixed and analyzed by confocal microscopy. Scale bar, 5 μm. Three cells were randomly selected for statistical analysis. Pearson's correlation coefficient (RIOK3 and TBK1) reflects the co-localization between the two. (G) IB analysis of proteins in EPC cells transfected with indicated

plasmids (1 μg each) for 24 h. (H and I) IB analysis of EPC cells transfected with specific plasmids (1 μg each) and either treated with poly I:C (0.5 μg) or infected with SVCV (MOI = 1). (J) Transfect 1 μg RIOK3-HA (or empty vector) and 1 μg TBK1-mCherry into EPC cells for 24 h. Then, fix the cells and analyse them via confocal microscopy. Scale bar: 100 μm.

5. RIOK3 degrades TBK1 via p62-dependent selective autophagy

To investigate the mechanism of RIOK3-mediated TBK1 degradation, we examined potential protein degradation pathways. The autophagy inhibitor chloroquine (CQ) rescued TBK1 levels, implicating autophagy in this process (Figure 5A). We next asked whether TBK1 itself induces autophagy. TBK1 expression did not increase LC3-II levels even in the presence of CQ (Figure 5B and C), nor did it induce LC3-GFP puncta formation (Figure 5E) or autophagosome structures, as observed by transmission electron microscope (TEM) (Figure 5G). In contrast, co-expression of RIOK3 and TBK1 increased LC3-II accumulation under CQ treatment (Figure 5D), promoted LC3-GFP puncta assembly (Figure 5F), and led to the appearance of autophagosome-like structures (Figure 5G). To investigate their roles in RIOK3-mediated TBK1 degradation, we constructed shRNAs targeting these three genes and validated their knockdown efficiency (Figure 5I). Further IB analysi revealed that only p62 overexpression enhanced RIOK3-mediated TBK1 degradation, while NBR1 and TOLLIP showed no significant effect (Figure 5J). Consistent with this, *p62* knockdown partially reversed RIOK3-mediated TBK1 degradation, whereas knocking down *nbr1* or *tollip* had no discernible impact (Figure 5K). Consistently, p62 suppressed TBK1-induced IFN activation, which was rescued upon p62 knockdown (Figure 5L). These data indicate that RIOK3 promotes autophagic degradation of TBK1 in a p62-dependent manner.

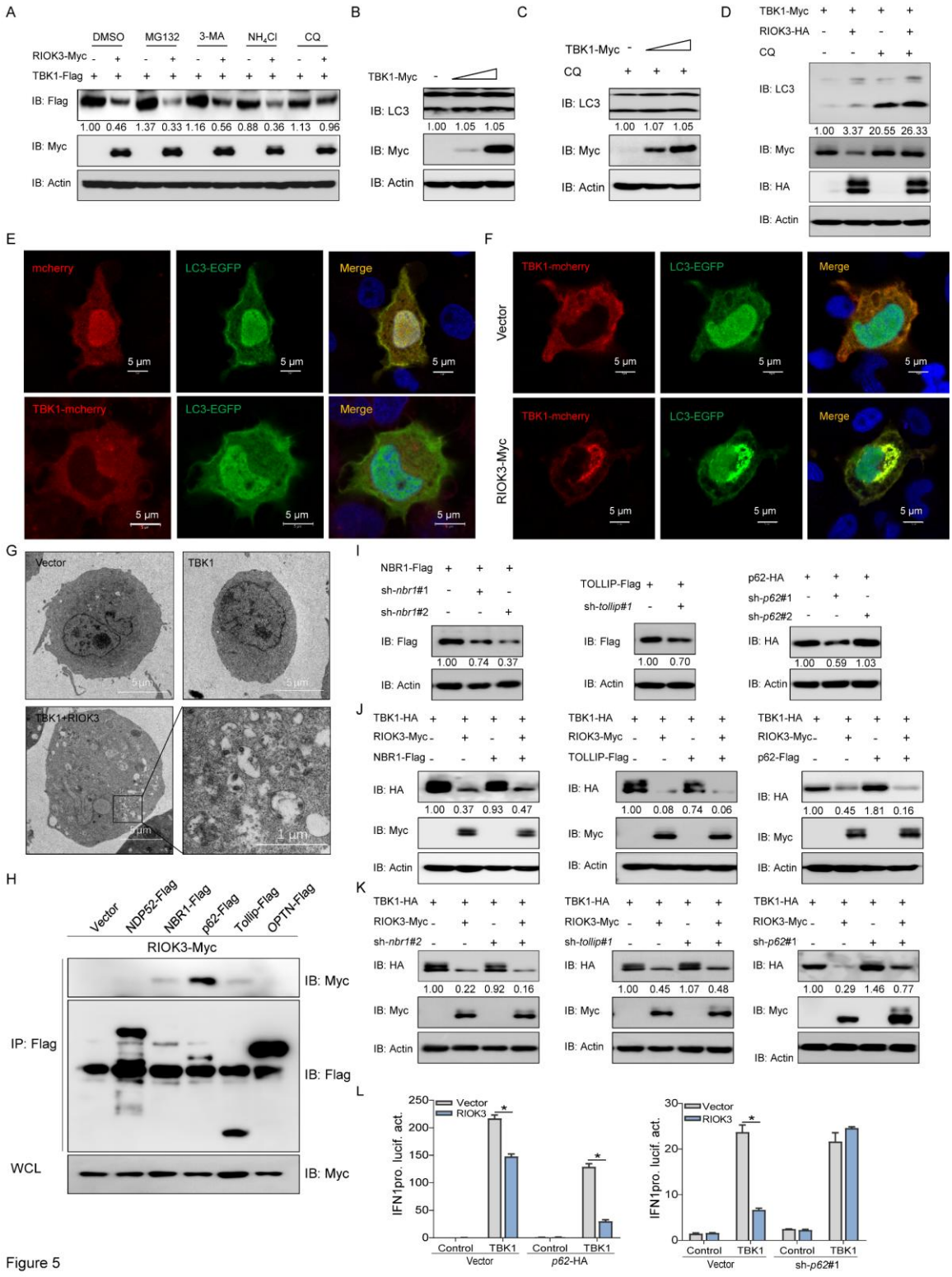

Figure 5

Figure 5. RIOK3 degrades TBK1 through the p62-mediated selective autophagy pathway. (A) EPC cells were transfected with the indicated plasmids (1 μg each). 18 h after transfection, cells were treated with

DMSO, MG132 (20 mM), 3-MA (2 mM), NH_4Cl (20 mM), or CQ (100 mM) for 6 h, followed by IB analysis. (B, I-K) EPC cells cultured in 6-well plates were transfected with the plasmids (1 μg each) and analyzed for IB after 24 h. (C) EPC cells were ctransfected with TBK1-Myc (0 μg, 1 μg, 2 μg). After 18 h of transfection, cells were treated with CQ (100 mM) for 6 h, followed by IB analysis. (D) EPC cells were co-transfected with the indicated plasmids (1 μg each). After 18 h of transfection, cells were treated with DMSO or CQ (100 mM) for 6 h, followed by IB analysis. (E and F) EPC cells were inoculated into 6-well plates with coverslips and transfected with the plasmids shown (1 μg each). After 24 h, the cells were fixed and analyzed by confocal microscopy (original magnification ×63). Scale bar, 5 μm. (G) EPC cells were cultured in a 6-well plate, transfected with the shown plasmid (1 μg each) and analyzed by TEM after 24 h. Enlarged sections show autophagic vesicles. Scale bar is 5 μm. (H) EPC cells cultured at 10 cm^2 were transfected with the plasmids shown (5 μg each) and immunoprecipitated with anti-Flag beads 24 h later. The immunoprecipitants and WCLs were then probed with Abs for IB analysis. (L) EPC cells were cultured in 24-well plates and transfected with the indicated plasmid (0.25 μg IFN1promoter, 0.25 μg TBK1-Myc, 0.25 μg p62-HA/sh-*p62*#1, 0.05 μg TK). 24 h after transfection, the activity of the cells was monitored by stimulating them with the dual-luciferase system.

6. SVCV P protein increases RIOK3 expression

In prior studies from our lab, we observed that suppression of IFN is a common viral immune evasion strategy. We therefore hypothesized that viruses may exploit RIOK3 mediated downregulation of IFN. To test this hypothesis, we performed the following analyses. As shown in Figure 6A, SVCV infection upregulated RIOK3 expression, but inactivated virus does not affect it. Co-IP assays revealed that RIOK3 specifically binds to the SVCV P protein, but not to N or G proteins (Figure 6B and 6C). Overexpression of the P protein increased RIOK3 levels (Figure 6D). Additionally, IF analysis showed a significant increase in green fluorescence of RIOK3 with the addition of the P protein (Figure 6E). Subsequently, we designed and constructed specific shRNA targeting the *p* gene and validated it. (Figure 6F). The results showed that *p* knockdown reduced RIOK3 expression (Figure 6G). Since RIOK3 is known to promote TBK1 degradation via autophagy, we investigated whether the P protein mediates TBK1 reduction through RIOK3. Overexpression of RIOK3 enhanced P-induced TBK1 degradation, whereas *riok3* knockdown attenuated this effect, indicating that P protein degrades TBK1 in a RIOK3-dependent manner (Figure 6H and 6I). Together, these results demonstrate that the SVCV P protein interacts with and upregulates RIOK3 to suppress TBK1 mediated antiviral signaling.

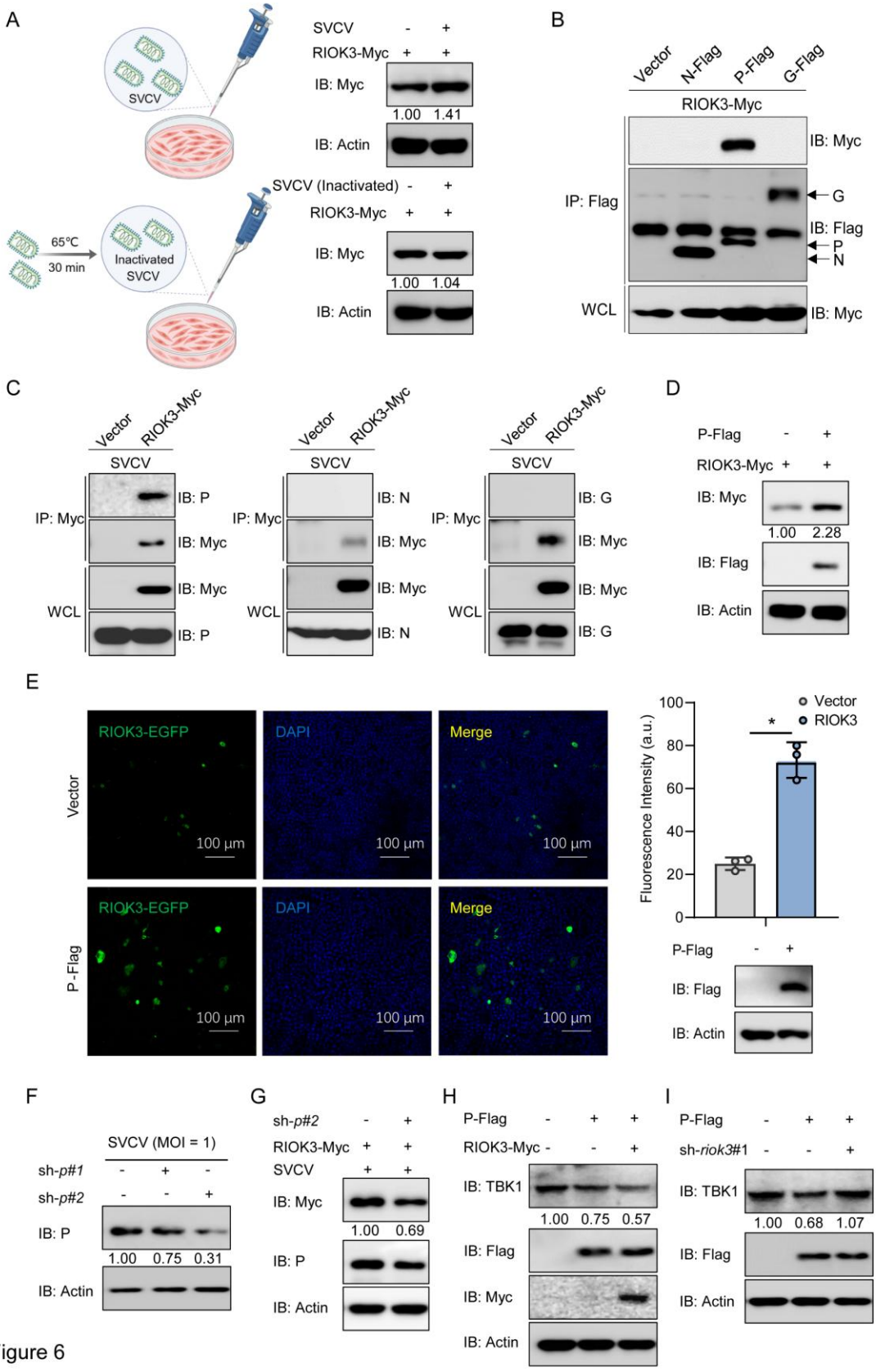

Figure 6

Figure 6. SVCV P increases RIOK3 expression. (A) EPC cells were seeded in 6-well plates and then transfected with 1 μg RIOK3-Myc. After 24 h, SVCV or inactivated SVCV (MOI = 1) was added, followed by IB analysis. Inactivated SVCV was obtained by heating SVCV at 65 °C for 30 min. (B) EPC cells were cultured in 10 cm^2 dishes and transfected with the described plasmids (5 μg each). 24 h later, cell lysates were IP using an anti-Flag affinity beads. The immunoprecipitants and WCLs were then probed with Abs IB. (C) EPC cells seeded in 10 cm^2 dishes were transfected with RIOK3-Myc (5 μg). After 24 h, the earlier co-transfected cells were infected with SVCV (MOI = 1); 24 h later, cell lysates were IP with anti-Myc affinity beads. The immunoprecipitants and WCLs were then probed with Abs IB. (D) IB analysis of EPC cells seeded in 6-well plates and transfected with the illustrated plasmid (1 μg each). (E) EPC cells were transfected with the plasmids shown (1 μg each) for 24 h. Cells were then fixed and analyzed by confocal microscopy. Scale bar, 100 μm. (F and G) EPC cells were seeded in 6-well plates and then transfected with the corresponding plasmids (1 μg each). After 24 h, SVCV (MOI = 1) was added, followed by IB analysis. (H and I) EPC cells cultured in 6-well plates were transfected with the plasmids (1 μg each) and analyzed for IB after 24 h.

7. P increases RIOK3 by enhancing TRIM11-mediated K63-type polyubiquitination

To elucidate the mechanism by which the P protein upregulates RIOK3, protein stability was assessed using cycloheximide (CHX). RIOK3 stability was enhanced in the presence of the P protein, but reduced upon knockdown of *p* (Figure 7A). Ubiquitination assays showed that the P protein promotes ubiquitination of RIOK3 (Figure 7B). Given that polyubiquitin chains linked to K63 are known to enhance protein stability, we examined ubiquitination using K63 specific ubiquitin mutants. Overexpression of the P protein increased levels of wild type ubiquitin (Ub-WT) and the K63 only mutant (Ub-K63O), but decreased that of the K63R mutant (Figure 7C and 7D), indicating that RIOK3 ubiquitination depends on K63. Mass spectrometry identified K318 as a putative ubiquitination site (Figure 7E). A K318R point mutation abolished the stabilizing effect of the P protein on RIOK3 (Figure 7F) and prevented Ub-WT and Ub-K63O ubiquitination (Figure 7G). Based on literature review and Co-IP results (32), TRIM11 exhibits binding to both RIOK3 and P (Figure 7H and 7I). Therefore, TRIM11 is selected as the potential E3 ubiquitin ligase. Domain mapping using BBOX and SPRY deletion constructs revealed that the SPRY domain of TRIM11 is necessary for binding to RIOK3 or P (Figure 7J–7L). TRIM11 enhances P-mediated upregulation of RIOK3 (Figure 7M). Constructed shRNAs targeting *trim11* and validated knockdown efficiency (Figure 7N). IB results showed that knockdown of *trim11* attenuated P

protein-mediated increase in RIOK3 (Figure 7O). Furthermore, TRIM11 enhanced Ub-WT and Ub-K63O ubiquitination of RIOK3 (Figure 7P), which was reduced in *trim11* knockdown cells (Figure 7Q). These results establish TRIM11 as the essential E3 ligase facilitating P induced RIOK3 stabilization.

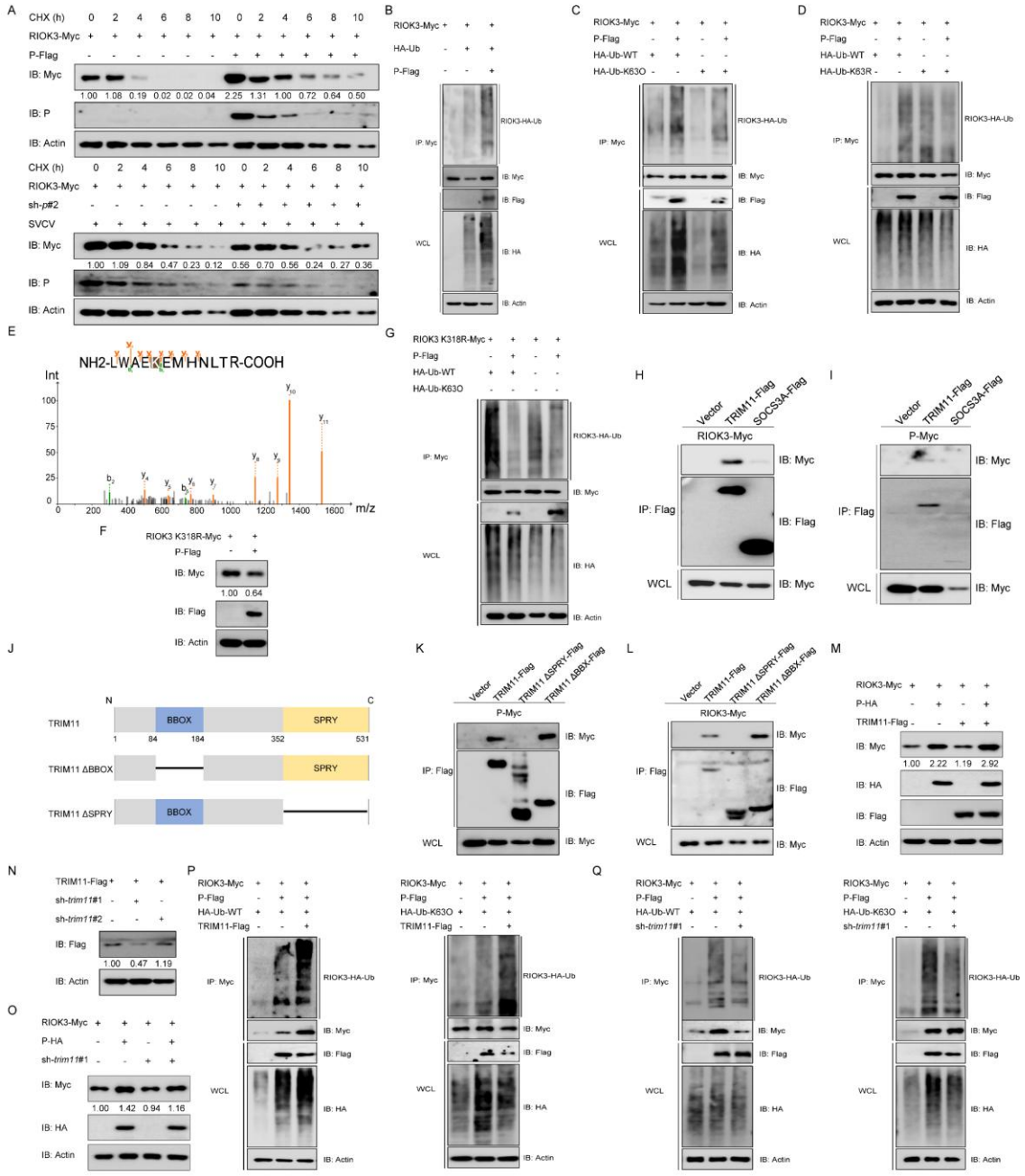

Figure 7

Figure 7. P increases RIOK3 by enhancing TRIM11-mediated K63-type polyubiquitination. (A) IB analysis of proteins in EPC cells transfected with indicated plasmids (1 μg each) for 18 h, then treated with CHX for 2 h, 4 h, 6 h, 8 h, and 10 h. (B-D, G, P and Q) EPC cells were seeded in 10 cm² culture dishes, transfected with the indicated plasmid (3 μg each), and subjected to RIOK3 ubiquitination detection after 24 h. (E) Mass spectrometry analysis of a peptide derived from ubiquitinated RIOK3-Myc. (F, M-O) EPC cells cultured in 6-well plates were transfected with the plasmids (1 μg each) and

analyzed for IB after 24 h. (H, I, K, L) EPC cells were cultured in 10 cm^2 dishes and transfected with the described plasmids (5 μg each). 24 h later, cell lysates were IP using an anti-Flag affinity beads. The immunoprecipitants and WCLs were then probed with Abs IB. (J) Schematic representation of full-length TRIM11 and its mutants.

In summary, this study reveals a cryptic immune evasion mechanism whereby SVCV upregulates the host factor RIOK3, a negative regulator of TBK1, thereby suppressing IFN production and facilitating viral proliferation (Figure 8).

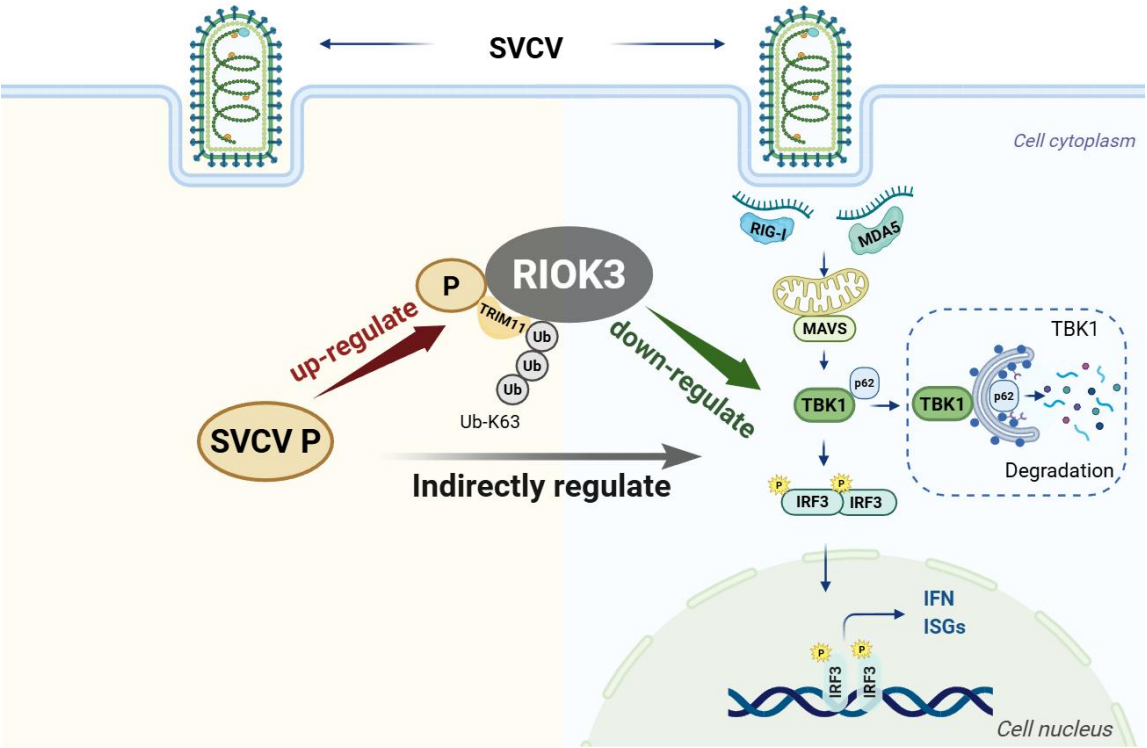

Figure 8. A model for a novel mechanism of immune escape by SVCV using the host IFN negative regulator molecule RIOK3.

Discussion

Fish viruses are notable among vertebrate viruses for their remarkably rapid replication kinetics, often reaching peak titers and causing host death within days post-infection (33). Whereas some mammalian virulent viruses, such as Ebola and Rabies, cause death within approximately one week of symptom onset, and others such as HIV or HBV cause mortality over years, common

351 piscine viruses like SVCV and GCRV can induce mortality within just 2–3 days (34). The
352 mechanisms underlying this extreme replicative efficiency have remained unclear. Our study
353 elucidates a highly efficient and subtle immune evasion strategy, providing new insights into viral
354 pathogenesis in fish and potentially broader perspectives on the evolution of viral virulence
355 strategies.

356 RIOK3, a member of the conserved RIO kinase family, functions in apoptosis and ribosome
357 quality control, with emerging roles in innate immunity(23, 25). In mammals, there are conflicting
358 reports regarding whether RIOK3 promotes or inhibits IFN responses via the RLR pathway (26,
359 27). Although previous reports have indicated that members of the fish RIO family possess similar
360 negative regulatory capabilities for IFN, the specific mechanisms underlying this phenomenon
361 remain unclear (29, 35). Here, we definitively show that fish RIOK3 acts as an IFN negative
362 regulator by mediating TBK1 degradation via the selective autophagy receptor p62. This functional
363 conservation across evolution is likely facilitated by high sequence and structural similarity,
364 exemplified by the 88.08% amino acid identity between fish and human RIOK3. Although a direct
365 interaction between human RIOK3 and TBK1 remains unconfirmed, the high degree of
366 conservation shared by TBK1, which exhibits 92.07% identity between these species, suggests
367 potential functional parallels and merits future investigation.

368 RIOK3 serves as a multifunctional suppressor of the IFN response, capable of inhibiting MDA5
369 and mediating TBK1 degradation. Such multiplexing allows viruses that target RIOK3 to disrupt
370 multiple nodes within the RLR pathway simultaneously with singular efficiency. Such a strategy
371 proves particularly advantageous for viruses, which possess limited genomic resources and must
372 evade host immunity optimally. First, targeting a single host factor significantly increases viral
373 protein efficiency. For example, SARS-CoV-2 requires at least four proteins, such as Nsp6, ORF7b,
374 Nsp13 and Nsp15, to inhibit MAVS and TBK1 separately (36). In contrast, SVCV utilizes only
375 one viral protein, the P protein, which upregulates RIOK3 to inhibit both MDA5 and TBK1

concurrently. Such resource economy enables the virus to allocate more resources toward virion assembly rather than deploying multiple proteins for host factor disruption. Second, the indirect mechanism is inherently stealthier. By enhancing the function of an endogenous host negative regulator, the virus avoids recognition as a foreign threat, thereby potentially mitigating the activation of robust host alarm systems or compensatory immune pathways. The cellular consequences of directly destroying a host protein versus coopting its physiological negative regulation are profoundly different. Direct viral cleavage of MAVS by poliovirus 3C protease or HCV NS3 4A protease inhibits IFN but generates aberrant fragments perceived as danger signals, potentially triggering inflammasome activation and apoptosis (37). In contrast, host mediated degradation of MAVS via ubiquitination by MARCH5, autophagy involving the ATG5 ATG12 conjugate, or proteolytic cleavage by caspases such as caspase 3, 6 and 8, is perceived as physiological regulation and does not typically induce inflammatory cascades (38–40).

The existence of direct evidence for immune evasion through the upregulation of interferon negative regulators in mammalian viruses remains limited, though scattered studies provide suggestive clues. For instance, hepatitis B virus (HBV) has been observed to persistently activate STAT3, a known negative regulator of IFN signaling, to facilitate hepatocarcinogenesis (41). In a similar manner, human cytomegalovirus (HCMV) encodes pUL97, which upregulates SOCS3, another key suppressor of IFN responses, leading to impairments in neural progenitor cells (42). It is conceivable that HBV and HCMV may exploit the upregulation of STAT3 and SOCS3, respectively, to indirectly inhibit IFN signaling, a hypothesis that awaits experimental confirmation. In summary, the present study demonstrates that the SVCV phosphoprotein induces upregulation of the host negative regulator RIOK3 as a refined immune evasion strategy. This mechanism acts subtly to evade host surveillance and prevents intense cellular responses that could otherwise reduce viral replication window. Furthermore, by leveraging the capacity of RIOK3 to inhibit multiple signaling intermediates, SVCV achieves potent and broad suppression of antiviral

401 defenses. This finding underscores the sophisticated adaptability and strategic resourcefulness
402 employed by viruses, including those infecting lower vertebrates, to subvert host immune
403 mechanisms.

404 ## Materials and Methods

405 ### 1. Ethics statement

406 All animal experiments conducted as part of this study were carried out in accordance with
407 the relevant ethical guidelines and have been approved by the Ethics Committee for Animal
408 Experiments of the Institute of Hydrobiology, Chinese Academy of Sciences (Approval No. 2024-
409 026).

410 ### 2. Fish

411 The WT zebrafish (*Danio rerio*) was obtained from the Chinese Zebrafish Resource Centre
412 (CZRC). The *riok3*$^{-/-}$ mutant zebrafish were obtained through the use of CRISPR-Cas9 technology.
413 The zebrafish were cultivated and reared in accordance with the established standard procedures.
414 The identification of knockout fish involves procedures such as tail DNA extraction, PCR
415 amplification, and sequencing. The sequencing service was provided by Wuhan Aikangjian
416 Biotechnology Co., Ltd. The zebrafish, which had reached approximately 2.5 months (0.4 ± 0.1 g)
417 after the hatching of mature zebrafish individuals, were employed for the experiments. In
418 accordance with the national animal welfare requirements, all zebrafish utilized in the experiments
419 were required to undergo a period of more than two weeks of acclimatization in the laboratory.
420 Their health status was evaluated and deemed satisfactory prior to their utilization in the
421 experiments.

422 ### 3. Zebrafish infection and samplings

SVCV (5×10^8 $TCID_{50}$/mL, 5 μL per group) was injected intraperitoneally into 3-month zebrafish, with zebrafish injected with PBS serving as controls. 48 h after SVCV infection, the liver, spleen and heart tissues were dissected and removed using dissecting forceps and scissors. The liver and spleen were used for qRT-PCR and IB analysis, while heart tissue was used to determine the viral titer.

4. Cells and viruses

The epithelioma papulosum cyprini (EPC) cells and Grass carp ovary (GCO) cells were obtained from the Chinese Type Culture Collection (CCTCC) and cultured in 199 medium (Invitrogen) at 28°C with 5% CO_2. Zebrafish liver (ZFL) cells were procured from the American Type Culture Collection (ATCC) and cultured in Ham's F-12 medium (Invitrogen) at 28°C with 5% CO_2. GiCB cells from Dr. Ling-Bing Zeng (Yangtze River Fisheries Research Institute) were cultured at 28°C, 5% CO_2 in 199 added 10% FBS. The RNA virus SVCV was propagated as follows: EPC cells, grown at 28°C, were inoculated with SVCV (MOI = 1). Once the cells exhibited CPE, cell cultures containing SVCV were subjected to centrifugation at 4000 *g* for 20-30 min to remove cellular debris. The resulting supernatant was stored at -80°C until use.

5. Proteomics analysis and parallel reaction monitoring (PRM) experiments

TMT-labeled peptides were separated by high-pH reverse-phase HPLC into nine fractions, vacuum-dried, and resuspended. Separation was performed using an EASY-nLC 1200 system (Thermo Fisher) with acetonitrile gradient elution. Mass spectrometry analysis was performed on an Orbitrap instrument: full scan resolution 120,000 (m/z 350–1600), HCD fragmentation (NCE 28%), dynamic exclusion 30 seconds. Identification and quantification were performed using MaxQuant (v1.6.3.4) against the Pimephales promelas protein database, with TMT 6-plex labeling quantification. Data were normalized using Perseus (v1.5.6.0), and differentially expressed proteins were assessed via t-tests and coefficient of variation (CV) (fold change $\geq$1.2 or $\leq$0.83, $p < 0.05$, CV

447 < 20%). For PRM analysis, trypsin-digested peptides were separated using the EASY-nLC 1000
448 system. Data were acquired in PRM mode on an Orbitrap mass spectrometer, with Skyline
449 (v3.5.1.9942) performing targeted quantification and peak validation. The MS proteomics data
450 have been submitted to the iProX database (www.iprox.cn), with the dataset identifier
451 IPX0013488000.

452 **6. Plasmid construction and reagents**

453 The sequence of zebrafish RIOK3 (GenBank accession number: NM_001003614.2) was
454 downloaded from the NCBI (National Center for Biotechnology Information) website
455 (http://www.ncbi.nlm.nih.gov/). RIOK3 was amplified by polymerase chain reaction (PCR) using
456 cDNA from zebrafish tissue as a template and simultaneously ligated into pCMV-Myc (Clontech),
457 pCMV-HA (Clontech), and pcDNA3.1(+) (Invitrogen) expression vectors. In addition, zebrafish
458 MAVS (NM_001080584.2), and TBK1 (NM_001044748.2) were cloned into pCMV-Myc,
459 pCMV-HA, and pCMV-Tag2C vectors, respectively. The sequences of the IFN1promoter (derived
460 from zebrafish) and ISRE are detailed in Supporting Information Text 1. in the dual luciferase assay
461 were constructed according to the pGL3-Basic luciferase reporter programme (Promega), and the
462 pRL-TK vector was purchased from Promega. For subcellular localization experiments, zebrafish
463 RIOK3 was constructed on the pEGFP-N3 vector (Clontech) and zebrafish TBK1 was constructed
464 on the pCS2-mCherry vector (Clontech). The ubiquitin mutant plasmids Ub-K63O and Ub-K63R
465 were ligated into the pCMV-HA vector. The primers and their sequences used in this study are
466 shown in Supporting Information Table S2, and all constructed expression vectors were confirmed
467 by sequencing. Polyinosinic-polycytidylic acid (poly I:C) was procured from Sigma-Aldrich and
468 utilized at a final concentration of 1 μg/μl. MG132 (Cat. No. M7449), 3-Methyladenine (3-MA)
469 (Cat. No. M9281), and CQ (Cat. No. C6628) were also sourced from Sigma-Aldrich. CHX (NSC-
470 185) were acquired from Selleck.

7. Luciferase activity assay

EPC cells were cultured overnight in 24-well plates and then transfected with the luciferase reporter plasmid and the expression plasmid shown in the text. To ensure that the same total amount was transfected in each well, pcDNA3.1(+) empty vectors were made up using FishTrans (Masonite Biotech) transfection reagents. 24 h after transfection, poly I:C was transfected, and 48 h after transfection, cells were washed with phosphate-buffered saline (PBS) and luciferase activity was measured using the Dual-Luciferase Reporter Analysis System (Promega). Firefly luciferase activity was normalized according to Renilla luciferase activity.

8. Transient transfection and virus infection

ZFL cells , GCO cells and GiCB cells are typically transfected in 6-well plates, whereas EPC cells are usually transfected in both 6-well and 24-well plates. The transfection was conducted using FishTrans transfection reagents. Antiviral assays were conducted using EPC cells cultured in 24-well plates, transfected with 0.5 μg RIOK3-Myc or an empty vector, and infected with SVCV (MOI = 1) 24 h later. Supernatants were collected from the cells 24 or 48 h after infection. The cells were fixed with 4% PFA and subsequently stained with 1% purple crystal. Following staining, the cells are prepared for observation of CPE. The viral titer in the supernatant is quantified using the method of Reed and Muench. The viral titer is determined in a 96-well plate by first serially diluting the supernatant three-fold and adding it to the EPC cells. Following a 48 or 72 h period during which the cells cease to develop lesions, the culture medium is discarded, the cells are rinsed with PBS, fixed in 4% PFA, and stained with 1% crystalline violet. The viral titer was determined to be 50% of the infectious dose to the cells ($TCID_{50}$/mL).

9. RNA extraction, reverse transcription, and quantitative PCR (qRT-PCR)

Total RNA was extracted using the TRIzol method (Invitrogen), and genomic DNA was digested with RNase-free DNase (Takara). cDNA was synthesized using the GoScript Reverse

Transcription System (Takara) in accordance with the instructions provided, and the PCR process was carried out using a fast SYBR green PCR master mix (Bio-Rad) in a CFX96 real-time system. qRT-PCR was conducted on a CFX96 real-time system using a fast SYBR green PCR master mix (Bio-Rad), with *β-actin* serving as the internal reference gene. The procedure was as follows: the first step was conducted at 95°C for 5 min, the second step was comprised of 40 cycles. The temperature was maintained at 95°C for 20 s, 60°C for 20 s, and 72°C for 30 s. The gene was employed as the internal reference gene, and *β-actin* was utilized for cDNA synthesis. The relative fold changes were calculated using the $2^{-\Delta\Delta Ct}$ method, with the control group serving as the reference point.

10. RNAi experiments

Primers for short hairpin RNA (shRNA) of RIOK3/P/TRIM11 were designed from the website (http://rnaidesigner.thermofisher.com/rnaiexpress/) and subsequently cloned into the PLKO.1-TRC vector. The shRNA was transfected into EPC cells cultured in 6-well plates, and the transfection reagents were used with FishTrans, with sh-NC serving as the negative control. The primer sequences are presented in Supporting Information Table S2.

11. Co-IP assay

EPC cells were cultured in 10 cm^2 dishes and transfected with 10 μg of the plasmid depicted in the accompanying figure. 24 h later, the medium was aspirated and the cells were washed with PBS. Subsequently, the cells were rapidly lysed with lysate for a period of 1-2 h. The composition of the lysate is as follows: The lysis buffer comprised 1% NP-40, 1 mM NaF, 50 mM Tris-HCl (pH 7.4), 1 mM EDTA, 150 mM NaCl, 1 mM sodium orthovanadate [Na_3VO_4], 1 mM phenylmethylsulfonyl fluoride (PMSF), 0.25% sodium deoxycholate, and a protease inhibitor mixture (Sigma-Aldrich, MO, USA). Subsequently, the lysate was transferred to a new centrifuge tube and subjected to centrifugation at 12,000 *g* for 15 min at 4°C, with the objective of removing

519 cell debris. Subsequently, the supernatant was transferred to a 1.5 mL centrifuge tube containing
520 20 μL of anti-Myc/Flag affinity beads (Sigma-Aldrich, MO, USA) and incubated at 4°C overnight.
521 On the following day, the precipitate was collected by centrifugation at 5,000 *g* for one minute,
522 washed three times with lysis buffer, and finally resuspended in 100 μL of sodium dodecyl sulphate
523 (SDS) sample buffer. It was then boiled at 100°C for 10 min. The immunoprecipitates and whole
524 cell lysates (WCLs) were subjected to IB with the specified antibodies.

525 **12. *In vivo* ubiquitination assay**

526 The cells were initially lysed with RIPA lysate containing 1% SDS, denatured by boiling at
527 100°C for 10 min, and diluted with lysis buffer until the concentration of SDS was 0.1%. The
528 diluted supernatant was incubated with 15-20 μL of anti-Flag affinity beads (Sigma-Aldrich) at 4°C
529 overnight, with slow agitation. Subsequently, the immunoprecipitated proteins were washed 3
530 times with lysis buffer, centrifuged at 4°C for 1 min at 5000 *g* to collect the immunoprecipitated
531 proteins, and finally resuspended in 100 μL of 1× SDS sample buffer. The samples were then
532 analysed by IB.

533 **13. Immunoblot analysis**

534 The immunoprecipitates or WCL were initially separated by 8-15% SDS-PAGE gel and
535 subsequently transferred to a poly (vinylidene difluoride) (PVDF) membrane (Bio-Rad).
536 Subsequently, the PVDF membrane was closed in a solution of TBST (25 mM Tris-HCl, 150 mM
537 NaCl, 0.1% Tween 20, pH 7.5) containing 5% skimmed milk powder and stored at room
538 temperature for 1 h. The membranes were incubated overnight at 4°C with a diluted primary
539 antibody, washed three times with TBST, and then incubated with the corresponding secondary
540 antibody at room temperature for 1 h. The membranes were washed three times with TBST and
541 incubated for 1 h with the corresponding secondary antibody. The antibody was washed three times
542 with TBST, then stained with the immobilization Western chemiluminescent horseradish

peroxidase (HRP) substrate (Millipore) and developed with the TOUCH IMAGER (E-Blot). The antibodies and their dilution ratios are as follows: anti-Flag/HA (Sigma Aldrich) 1:3000; anti-Myc (Santa Cruz Biotechnology) 1:3000; anti-N/P/G (1:2000), anti-TBK1 (1:2000), and anti-IFN (1:500) were all prepared in our laboratory. The HRP-coupled anti-rabbit IgG or anti-mouse IgG (Thermo Scientific) was used at a dilution of 1:5000, while the anti-β-Actin (Cell Signal Technology) was diluted 1:10,000.

14. Fluorescent microscopy

A coverslip was placed in a 6-well plate, and EPC cells were subsequently cultured in it and transfected with the appropriate plasmid 24 h later. Following a 24 h transfection period, the plates were washed three times with PBS and fixed with 4% PFA for 1 h. After PBS washing, the plates were stained with 4',6-diamidino-2-phenylindole (DAPI) (1 μg/mL; Beyotime) for 8 min. Subsequently, the coverslips were affixed to the slides, imaged, and photographed with a confocal microscope (×63 immersion lens; SP8; Leica).

15. Histopathology

48 h after intraperitoneal challenge with SVCV, liver and spleen tissues were collected from the control and infected groups (n = 5 in each group) and fixed overnight in 10% phosphate-buffered formalin. The samples then underwent graded ethanol dehydration, paraffin embedding and serial sectioning at a thickness of 5 μm. Three non-overlapping sections per tissue type and per fish were randomly selected for haematoxylin and eosin (H&E) staining. The tissue lesions were observed under a light microscope and analysed using Aperio ImageScope software.

16. Transmission electron microscopy (TEM)

EPC cells cultured in 6-well plates were transfected with the plasmids indicated for a period of 24 h using FishTrans (Masonite Biotech). The cells were then washed three times with PBS,

trypsinised and transferred to a centrifuge tube, before being centrifuged at 2000 g for five minutes in order to collect the cell sediment. The cells were subsequently resuspended in 2.5% glutaraldehyde in 0.075 mol/L phosphate buffer (pH 7.4) and pretreated for 4 h at 4°C. Subsequently, the cells were treated with 0.075 mol/L phosphate buffer (pH 7.4) for 4 h at 4°C. Subsequently, the cells were washed three times with a solution comprising 0.075 mol/L phosphate and 0.19 mol/L sucrose, and fixed with 0.24 mol/L phosphate buffer (pH 7.4) containing 1% OsO_4 for a period of 2 h. Ultrathin sections (74 nm) were prepared using a microtome (UC7; Leica) and mounted on copper channel grids. The prepared sections were subjected to a double staining procedure, wherein they were treated with a solution of 3% uranyl acetate and lead citrate for a period of 10 min. Thereafter, the sections were observed under a transmission electron microscope (HT7700; Hitachi).

17. Statistics analysis

Kaplan-Meier survival curves were plotted and analyzed by log-rank tests for zebrafish survival experiments. The resulting histograms represent the results of three independent experiments, with each point in the bitmap representing an independent biological replicate. Unpaired Student's t-tests were used for statistical analyses, with data expressed as mean ± standard error of the mean (SEM). * $p < 0.05$ was considered statistically significant. In quantitative protein analysis, use ImageJ software (National Institutes of Health) to analyse SDS-PAGE photographs. Convert the image to 8-bit grayscale, perform background subtraction and invert the image. Use the rectangle tool to outline the region containing the target protein band. The software will then read the integrated density within the outlined region as a grayscale value, which can be used to compare protein yield differences under different conditions. Target protein signals were normalised against the β-actin signal from the corresponding sample.

Acknowledgments

We thank Fang Zhou (Analysis and Testing Center, IHB, CAS) for assistance with confocal microscopy analysis and Feng Xiong (China Zebrafish Resource Center, IHB, CAS) for assistance with qRT-PCR analysis. We thank Xin Wang and Guang-Xin Wang (Analysis and Testing Center, IHB, CAS) for assistance with Histopathology. We thank Dr. Yan-Yi Wang (Wuhan Institute of Virology, Chinese Academy of Sciences) for providing Ub-related plasmids (HA-Ub-WT, HA-Ub-K63R, and HA-Ub-K63O).

Funding

This work was supported by Strategic Priority Research Program of the Chinese Academy of Sciences (XDB0730300), the project of cross-disciplinary research team of State Key Laboratory of Breeding Biotechnology and Sustainable Aquaculture (2024BBSA09), the National Excellent Youth Science Fund (32322086), and the National Natural Science Foundation of China (32173023).

Author Contributions

Feng Ge, Shun Li and Li Zhou designed research; Can Zhang, Long-Feng Lu, Chu-Jing Zhou, Ming-Kun Yang, Hui-Lin Li, Bao-Jie Cui, Xiao Xu, and Meng-Ze Tian performed research; Can Zhang, Zhuo-Cong Li, Yang-Yang Wang, Zhen-Qi Li, Dan-Dan Chen and Feng Xiong analyzed data; Can Zhang, Long-Feng Lu, Shun Li and Feng Ge wrote the paper.

Competing Interest Statement

The authors have no financial conflicts of interest.

References

1. S. Dupuis, *et al.*, Impaired response to interferon-alpha/beta and lethal viral disease in human STAT1 deficiency. *Nat Genet* **33**, 388–391 (2003).

2. J. E. Durbin, R. Hackenmiller, M. C. Simon, D. E. Levy, Targeted disruption of the mouse Stat1 gene results in compromised innate immunity to viral disease. *Cell* **84**, 443–450 (1996).
3. A. García-Sastre, Ten Strategies of Interferon Evasion by Viruses. *Cell Host Microbe* **22**, 176–184 (2017).
4. H.-R. Lee, M. H. Kim, J.-S. Lee, C. Liang, J. U. Jung, Viral interferon regulatory factors. *J Interferon Cytokine Res* **29**, 621–627 (2009).
5. S. Li, L.-F. Lu, C. Zhang, The LxIS motif is the language between virus and host RLRs: From fish to mammalian viruses. *Water Biology and Security* **3**, 100246 (2024).
6. X. Liu, D. Main, Y. Ma, B. He, Herpes Simplex Virus 1 Inhibits TANK-Binding Kinase 1 through Formation of the Us11-Hsp90 Complex. *J Virol* **92**, e00402-18 (2018).
7. X. Zhang, *et al.*, SARS-CoV-2 Nsp8 suppresses MDA5 antiviral immune responses by impairing TRIM4-mediated K63-linked polyubiquitination. *PLoS Pathog* **19**, e1011792 (2023).
8. L. F. Lu, *et al.*, Fish herpesvirus KLP manipulates Beclin1 to selectively degrade MITA through a precise autophagic manner for immune evasion. *Water Biology and Security* **2**.
9. L.-F. Lu, *et al.*, Grass Carp Reovirus VP41 Targets Fish MITA To Abrogate the Interferon Response. *J. Virol.* **91**, e00390-17 (2017).
10. O. Takeuchi, S. Akira, Pattern Recognition Receptors and Inflammation. *Cell* **140**, 805–820 (2010).
11. S. Akira, S. Uematsu, O. Takeuchi, Pathogen Recognition and Innate Immunity. *Cell* **124**, 783–801 (2006).
12. J. Zheng, *et al.*, RIG-I-like receptors: Molecular mechanism of activation and signaling. *Adv Immunol* **158**, 1–74 (2023).
13. Y.-M. Loo, M. Gale, Immune signaling by RIG-I-like receptors. *Immunity* **34**, 680–692 (2011).
14. L. Wang, D. He, N. Satoh-Takayama, C. Zheng, J. Xing, Regulation of antiviral and antimicrobial innate immunity and immune evasion. *Cell Mol Life Sci* **82**, 326 (2025).

15. T. Blumer, M. Coto-Llerena, F. H. T. Duong, M. H. Heim, SOCS1 is an inducible negative regulator of interferon λ (IFN-λ)-induced gene expression in vivo. *J Biol Chem* **292**, 17928–17938 (2017).
16. R. Li, Y. Pan, D.-D. Shi, Y. Zhang, J. Zhang, PIAS1 negatively modulates virus triggered type I IFN signaling by blocking the DNA binding activity of IRF3. *Antiviral Res* **100**, 546–554 (2013).
17. K. Narayan, *et al.*, TRIM13 is a negative regulator of MDA5-mediated type I interferon production. *J Virol* **88**, 10748–10757 (2014).
18. S. Li, *et al.*, IFN regulatory factor 10 is a negative regulator of the IFN responses in fish. *J Immunol* **193**, 1100–1109 (2014).
19. L.-F. Lu, *et al.*, A novel role of Zebrafish TMEM33 in negative regulation of interferon production by two distinct mechanisms. *PLoS Pathog* **17**, e1009317 (2021).
20. J.-F. Gui, L. Zhou, X.-Y. Li, Rethinking fish biology and biotechnologies in the challenge era for burgeoning genome resources and strengthening food security. *Water Biology and Security* **1**, 100002 (2022).
21. Y.-W. Chen, W.-C. Ko, C.-S. Chen, P.-L. Chen, RIOK-1 Is a Suppressor of the p38 MAPK Innate Immune Pathway in Caenorhabditis elegans. *Front Immunol* **9**, 774 (2018).
22. N. LaRonde-LeBlanc, A. Wlodawer, A family portrait of the RIO kinases. *J. Biol. Chem.* **280**, 37297–37300 (2005).
23. K. Baumas, *et al.*, Human RioK3 is a novel component of cytoplasmic pre-40S pre-ribosomal particles. *RNA Biol.* **9** (2012).
24. L. Zhang, J. Flygare, P. Wong, B. Lim, H. F. Lodish, miR-191 regulates mouse erythroblast enucleation by down-regulating Riok3 and Mxi1. *Genes Dev.* **25**, 119–124 (2011).
25. J. Shan, *et al.*, RIOK3 interacts with caspase-10 and negatively regulates the NF-kappaB signaling pathway. *Mol Cell Biochem* **332**, 113–120 (2009).
26. Y. Shen, *et al.*, Riok3 inhibits the antiviral immune response by facilitating TRIM40-mediated RIG-I and MDA5 degradation. *Cell Reports* **35**, 109272 (2021).

664 27. K. Takashima, H. Oshiumi, H. Takaki, M. Matsumoto, T. Seya, RIOK3-Mediated
665 Phosphorylation of MDA5 Interferes with Its Assembly and Attenuates the Innate Immune
666 Response. *Cell Reports* **11**, 192–200 (2015).
667 28. J. Feng, *et al.*, RIOK3 is an adaptor protein required for IRF3-mediated antiviral type I interferon
668 production. *J Virol* **88**, 7987–7997 (2014).
669 29. X. Zhao, *et al.*, Yellow catfish RIO kinases (RIOKs) negatively regulate fish interferon-mediated
670 antiviral response. *Dev Comp Immunol* **142**, 104656 (2023).
671 30. W. Ahne, *et al.*, Spring viremia of carp (SVC). *Diseases of Aquatic Organisms* **52**, 261–272
672 (2002).
673 31. Y. Teng, *et al.*, Characterization of complete genome sequence of the spring viremia of carp virus
674 isolated from common carp (Cyprinus carpio) in China. *Arch Virol* **152**, 1457–1465 (2007).
675 32. L. Chen, G. Zhu, E. M. Johns, X. Yang, TRIM11 activates the proteasome and promotes overall
676 protein degradation by regulating USP14. *Nat Commun* **9**, 1223 (2018).
677 33. A. R. Wargo, R. J. Scott, B. Kerr, G. Kurath, Replication and shedding kinetics of infectious
678 hematopoietic necrosis virus in juvenile rainbow trout. *Virus Res* **227**, 200–211 (2017).
679 34. P. W. Li, J. Zhang, M. X. Chang, Structure, function and immune evasion strategies of
680 aquareoviruses, with focus on grass carp reovirus. *Reviews in Aquaculture* **16**, 410–432 (2024).
681 35. Q. Li, *et al.*, Black carp RIOK3 suppresses MDA5-mediated IFN signaling in the antiviral innate
682 immunity. *Dev Comp Immunol* **149**, 105059 (2023).
683 36. H. Fan, *et al.*, Strategies Used by SARS-CoV-2 to Evade the Innate Immune System in an
684 Evolutionary Perspective. *Pathogens* **13**, 1117 (2024).
685 37. A. Mukherjee, *et al.*, The Coxsackievirus B 3Cpro Protease Cleaves MAVS and TRIF to
686 Attenuate Host Type I Interferon and Apoptotic Signaling. *PLOS Pathogens* **7**, e1001311 (2011).
687 38. C. Li, *et al.*, E3 ubiquitin ligase MARCH5 positively regulates Japanese encephalitis virus
688 infection by catalyzing the K27-linked polyubiquitination of viral E protein and inhibiting
689 MAVS-mediated type I interferon production. *mBio* **16**, e00208-25.

690 39. Y. Chun, J. Kim, Autophagy: An Essential Degradation Program for Cellular Homeostasis and
691 Life. *Cells* **7**, 278 (2018).
692 40. P.-H. H. Cheung, *et al.*, Virus subtype-specific suppression of MAVS aggregation and activation
693 by PB1-F2 protein of influenza A (H7N9) virus. *PLoS Pathog.* **16**, e1008611 (2020).
694 41. K. Yuan, *et al.*, HBV-induced ROS accumulation promotes hepatocarcinogenesis through Snail-
695 mediated epigenetic silencing of SOCS3. *Cell Death Differ* **23**, 616–627 (2016).
696 42. X.-Z. Wang, *et al.*, Human cytomegalovirus pUL97 upregulates SOCS3 expression via
697 transcription factor RFX7 in neural progenitor cells. *PLoS Pathog* **19**, e1011166 (2023).
698